J. Fluid Mech. (1992), *vol.* 242, *pp.* 99–116
Printed in Great Britain

Two-dimensional instabilities of steady double-diffusive interleaving

By OLIVER S. KERR
School of Mathematics, University of Bristol, Bristol BS8 1TW, UK

(Received 14 March 1991 and in revised form 10 February 1992)

The stability of finite-amplitude double-diffusive interleaving driven by linear gradients of salinity and temperature is considered. We show that as the sinusoidal interleaving predicted by linear analysis grows to finite amplitude it is subject to instabilities centred along the lines of minimum vertical density gradient and maximum shear. These secondary instabilities could lead to the step-like density profiles observed in experiments. We show that these instabilities can occur for large Richardson numbers and hence are not driven by shear, but are driven, by double-diffusive effects.

1. Introduction

When a stratified body of fluid has lateral variations of both temperature and salinity it can often undergo instabilities that result in the formation of a series of almost horizontal convecting layers. Various configurations corresponding to this situation have been investigated experimentally, including applying temperature differences to stratified bodies of fluid at or between single or parallel boundaries (Thorpe, Hutt & Soulsby 1969; Chen, Briggs & Wirtz 1971; Wirtz, Briggs & Chen 1972; Chen & Skok 1974; Paliwal & Chen 1980*a*; Narusawa & Suzukawa 1981; Tanny & Tsinober 1988) or from point or line sources (Huppert & Turner 1980; Huppert & Josberger 1980; Tsinober, Yahalom & Shlien 1983). Instabilities that lead to layer formation are also observed at interfaces between bodies of fluid with similar vertical density gradients, but with lateral differences in composition (Ruddick & Turner 1979; Holyer *et al.* 1987). Similar instabilities can also be formed by the presence of sloping insulating boundaries (Linden & Weber 1977; Chen & Sandford 1977). In addition to the theoretical work carried out by some of these investigators there has been further analysis of the case of temperature differences applied at single or parallel boundaries (Hart 1971, 1973; Paliwal & Chen 1980*b*; Thangam, Zebib & Chen 1981; Kerr 1989, 1990, 1991).

Theoretical work has also been carried out on the effects of lateral compositional gradients on stratified fluids in the idealized case of uniform linear gradients in *all* directions, but with no horizontal density gradients (Stern 1967; Toole & Georgi 1981; Posmentier & Hibbard 1982; Holyer 1983; McDougall 1985). This work uses a variety of models for the fluxes of the heat and salt: vertical fluxes due to salt fingering (Stern and Posmentier & Hibbard), eddy-flux coefficients (McDougall) and molecular diffusivities (Holyer). In the latter case the fluid is always subject to instabilities if there are compensating horizontal temperature and salinity gradients. Similar results hold for other models of heat and salt fluxes provided the vertical gradients are such that small-scale convective mixing needed for these fluxes is sustained.

Holyer noted that the linear modes of her analysis also satisfied the fully nonlinear equations of motion. Hence a single unstable mode could grow exponentially to large amplitude and eventually result in there being density inversions in the fluid. It can be anticipated from this that the interleaving layers would themselves eventually become unstable. It is the purpose of this paper to investigate these secondary instabilities in order to find what form they would take, when they may be observed, and to explain some of the features observed in experiments. This investigation is comprised of a two-dimensional linear stability analysis of the interleaving layers. This analysis follows a similar line to Holyer (1984) in her analysis of the stability of long two-dimensional salt fingers.

In §2 we set out the governing equations for steady double-diffusive interleaving driven by linear temperature and salinity gradients and derive the perturbation equations for the investigation of their linear stability. Some results obtained from this stability analysis are presented in §3, together with a look at the asymptotic limit of relatively weak horizontal background gradients.

2. Perturbation equations

Double-diffusive interleaving occurs when a body of fluid with vertical temperature and salinity gradients is subjected to lateral temperature and salinity gradients. Here we consider the idealized problem where interleaving develops in a fluid with linear gradients in all directions. We set the temperature and salinity to

$$T(x,z,t) = T_0 + x\bar{T}_x + z\bar{T}_z + T'(x,z,t) \tag{2.1a}$$

and

$$S(x,z,t) = S_0 + x\bar{S}_x + z\bar{S}_z + S'(x,z,t), \tag{2.1b}$$

where $T_0, \bar{T}_x, \bar{T}_z, S_0, \bar{S}_x$ and $\bar{S}_z$ are all constants, T' and S' are two-dimensional perturbations to the background state, and x and z are the horizontal and vertical coordinates respectively. We assume that the density, ρ, depends linearly on the temperature and salinity:

$$\rho = \rho_0\{1-\alpha(T-T_0)+\beta(S-S_0)\}, \tag{2.2}$$

where α and β are positive constants.

Double-diffusive interleaving arises as an instability to an otherwise quiescent fluid and so we require that there is no net horizontal density gradient. This occurs when

$$\alpha\bar{T}_x = \beta\bar{S}_x. \tag{2.3}$$

Without loss of generality we choose the x-axis so that $\bar{S}_x$ is positive. Hence, for any given depth, the salinity increases as x increases.

Making the Boussinesq approximation, the equations for the perturbation stream function ψ', temperature, T', and salinity, S', of an incompressible fluid are

$$\frac{\partial\nabla^2}{\partial t}\psi' + J(\psi', \nabla^2\psi') = g\left(\alpha\frac{\partial T'}{\partial x} - \beta\frac{\partial S'}{\partial x}\right) + \nu\nabla^4\psi', \tag{2.4a}$$

$$\frac{\partial T'}{\partial t} + J(\psi', T') - \frac{\partial\psi'}{\partial z}\bar{T}_x + \frac{\partial\psi'}{\partial x}\bar{T}_z = \kappa_T\nabla^2 T', \tag{2.4b}$$

$$\frac{\partial S'}{\partial t} + J(\psi', S') - \frac{\partial\psi'}{\partial z}\bar{S}_x + \frac{\partial\psi'}{\partial x}\bar{S}_z = \kappa_S\nabla^2 S', \tag{2.4c}$$

where the velocity $$\boldsymbol{u}' = \left(-\frac{\partial \psi'}{\partial z}, \frac{\partial \psi'}{\partial x}\right) \tag{2.4d}$$

and the Jacobian is given by

$$J(A,B) = \frac{\partial A}{\partial x}\frac{\partial B}{\partial z} - \frac{\partial A}{\partial z}\frac{\partial B}{\partial x}. \tag{2.5}$$

The acceleration due to gravity is denoted by g, the kinematic viscosity by ν, the diffusivity of heat by κ_T, and the diffusivity of salt by κ_S.

If the Jacobian terms are dropped we obtain a linear set of equations with constant coefficients. Hence we can express any solution as a linear superposition of solutions of the form

$$(\psi', T', S') = \mathrm{Re}\{(\psi_0', T_0', S_0') \exp(\mathrm{i}\boldsymbol{k}\cdot\boldsymbol{x} + \lambda t)\}, \tag{2.6}$$

where ψ_0', T_0' and S_0' are complex constants, $\boldsymbol{k} = (k, m)$ is the wavenumber vector and λ is the growth rate, which may be complex. Holyer (1983) noted that if only one such mode existed, say the fastest growing mode, then it would be a solution of the fully nonlinear governing equations. When a single such mode is substituted into (2.4) we derive the dispersion relation

$$\begin{aligned}(\lambda+\nu\mu^2)(\lambda+\kappa_T\mu^2)(\lambda+\kappa_S\mu^2)\mu^2 + \lambda g(\alpha\bar{T}_z - \beta\bar{S}_z)k^2 \\ + k^2\mu^2 g\kappa_T\kappa_S\left(\frac{\alpha\bar{T}_z}{\kappa_T} - \frac{\beta\bar{S}_z}{\kappa_S}\right) + g\beta\bar{S}_x(\kappa_T-\kappa_S)\mu^2 km = 0,\end{aligned} \tag{2.7}$$

where $\mu = (k^2+m^2)^{\frac{1}{2}}$ is the wavenumber for this interleaving mode. We restrict ourselves to consideration of the direct modes of instability with λ real. Holyer noted that the direct modes of instability grew faster than the oscillatory modes except in the restricted case when $\bar{T}_z$ is negative, $\beta\bar{S}_z/\alpha\bar{T}_z$ lies between 1 and $(\sigma+1)/(\sigma+\tau)$ (defined in (2.10)), and $\beta\bar{S}_x/\alpha\bar{T}_z$ is small. In these cases the fastest growing modes have the ratio $m/k \ll 1$ and as such are nearly vertical. These instabilities will not concern us here.

The fastest growing modes also satisfy the extra constraints

$$\frac{\partial\lambda}{\partial k} = \frac{\partial\lambda}{\partial m} = 0. \tag{2.8}$$

By differentiating the characteristic equation (2.7) with respect to the wavenumber-vector components k and m we get two equations that are to be solved simultaneously with (2.7) to find the values of λ, k and m that correspond to the maximum growth rate. Following Holyer we non-dimensionalize these equations. We define

$$q = \frac{\lambda}{\kappa_T\mu^2}, \tag{2.9a}$$

and

$$H = \frac{g\beta\bar{S}_x}{\nu\kappa_T\mu^4}, \quad R_T = \frac{g\alpha\bar{T}_z}{\nu\kappa_T\mu^4}, \quad R_S = \frac{g\beta\bar{S}_z}{\nu\kappa_T\mu^4}, \tag{2.9b–d}$$

where H is the horizontal Rayleigh number and R_T and R_S are the vertical thermal and saline Rayleigh numbers. We have used here the lengthscale, $|\mu|^{-1}$, of the fastest growing modes of instability as the appropriate natural lengthscale.

We also define

$$\sigma = \frac{\nu}{\kappa_T}, \quad \tau = \frac{\kappa_S}{\kappa_T}, \tag{2.10}$$

where σ is the Prandtl number and τ the salt/heat diffusivity ratio.

The following non-dimensional equations relating q and m/k for the fastest growing mode to the Rayleigh numbers are obtained:

$$H = -\frac{2m}{k}\frac{1}{\sigma(1-\tau)}(q+\sigma)(q+1)(q+\tau), \tag{2.11a}$$

$$R_T = \frac{k^2+m^2}{k^2}\frac{q+1}{q\sigma(1-\tau)}\left[-q^3+q(\sigma\tau+\sigma+\tau)+2\sigma\tau+\frac{k^2-m^2}{k^2+m^2}q(q+\sigma)(q+\tau)\right], \tag{2.11b}$$

$$R_S = \frac{k^2+m^2}{k^2}\frac{q+\tau}{q\sigma(1-\tau)}\left[-q^3+q(\sigma\tau+\sigma+\tau)+2\sigma\tau+\frac{k^2-m^2}{k^2+m^2}q(q+\sigma)(q+1)\right]. \tag{2.11c}$$

In a physical problem we would not be able to calculate directly the three Rayleigh numbers from the background gradients, but only their ratios. From these ratios we can use the above equations to find q and the ratio m/k, and thence the Rayleigh numbers and the lengthscale of the instabilities.

Instead of investigating the stability of the fastest growing mode, we follow Holyer (1984) in her investigation of the stability of salt fingers by looking at the stability of modes with zero growth rate. The marginally stable interleaving layers that we choose to investigate are those that are parallel to the fastest growing layers. Having selected such a mode we can then give the intrusions arbitrary amplitude. We look at linear perturbations to these layers in order to investigate their stability. If the growth rate of these infinitesimal perturbations is larger than that of the fastest growing mode then these instabilities could be expected to manifest themselves in a physical situation.

We non-dimensionalize the variables in the governing equations with respect to the following:

$$x \text{ with respect to } |\mu|^{-1}, \tag{2.12a}$$

$$t \text{ with respect to } (\mu^2\kappa_T)^{-1}, \tag{2.12b}$$

$$\psi' \text{ with respect to } \kappa_T, \tag{2.12c}$$

$$T' \text{ with respect to } \nu\kappa_T|\mu|^3/(g\alpha), \tag{2.12d}$$

$$S' \text{ with respect to } \nu\kappa_T|\mu|^3/(g\beta). \tag{2.12e}$$

This gives the non-dimensional governing equations, after dropping the primes:

$$\frac{1}{\sigma}\left[\frac{\partial\nabla^2}{\partial t}\psi + J(\psi,\nabla^2\psi)\right] = \frac{\partial T}{\partial x} - \frac{\partial S}{\partial x} + \nabla^4\psi, \tag{2.13a}$$

$$\frac{\partial T}{\partial t} + J(\psi,T) + R_T\frac{\partial\psi}{\partial x} - H\frac{\partial\psi}{\partial z} = \nabla^2 T, \tag{2.13b}$$

$$\frac{\partial S}{\partial t} + J(\psi,S) + R_S\frac{\partial\psi}{\partial x} - H\frac{\partial\psi}{\partial z} = \tau\nabla^2 S. \tag{2.13c}$$

By the choice of the non-dimensionalizations for T and S the Rayleigh numbers R_T, R_S and H do not appear in the momentum equation, as is more common. This avoids possible problems associated with setting any of the Rayleigh numbers to zero.

The marginally stable solution we select is denoted by

$$\psi = -\hat{\psi}\cos(\hat{\boldsymbol{k}}\cdot\boldsymbol{x}), \quad T = \hat{T}\sin(\hat{\boldsymbol{k}}\cdot\boldsymbol{x}), \quad S = \hat{S}\sin(\hat{\boldsymbol{k}}\cdot\boldsymbol{x}), \tag{2.14a–c}$$

with

$$\hat{\boldsymbol{k}} = (\hat{k}, \hat{m}) \quad \text{and} \quad \hat{\mu}^2 = \hat{k}^2 + \hat{m}^2. \tag{2.14d,e}$$

For given ratio $\hat{m}/\hat{k}$, the coefficients $\hat{\psi}$, $\hat{T}$ and $\hat{S}$ and the wavenumber, $\hat{\mu}$, are related by

$$0 = \hat{k}(\hat{T}-\hat{S}) - \hat{\mu}^4\hat{\psi}, \tag{2.15a}$$

$$(\hat{m}H - \hat{k}R_T)\hat{\psi} = \hat{\mu}^2\hat{T}, \tag{2.15b}$$

and

$$(\hat{m}H - \hat{k}R_S)\hat{\psi} = \tau\hat{\mu}^2\hat{S}. \tag{2.15c}$$

The governing equations for the infinitesimal perturbations to this background state, $\tilde{\psi}$, $\tilde{T}$ and $\tilde{S}$ are

$$\frac{1}{\sigma}\left[\frac{\partial\nabla^2}{\partial t}\tilde{\psi} + \hat{\psi}\sin(\hat{\boldsymbol{k}}\cdot\boldsymbol{x})\left\{\hat{k}\left(\frac{\partial\nabla^2}{\partial z}\tilde{\psi} + \hat{\mu}^2\frac{\partial\tilde{\psi}}{\partial z}\right) - \hat{m}\left(\frac{\partial\nabla^2}{\partial x}\tilde{\psi} + \hat{\mu}^2\frac{\partial\tilde{\psi}}{\partial x}\right)\right\}\right] = \frac{\partial\tilde{T}}{\partial x} - \frac{\partial\tilde{S}}{\partial x} + \nabla^4\tilde{\psi}, \tag{2.16a}$$

$$\frac{\partial\tilde{T}}{\partial t} + \tilde{\psi}\sin(\hat{\boldsymbol{k}}\cdot\boldsymbol{x})\left(\hat{k}\frac{\partial\tilde{T}}{\partial z} - \hat{m}\frac{\partial\tilde{T}}{\partial x}\right) + \hat{T}\cos(\hat{\boldsymbol{k}}\cdot\boldsymbol{x})\left(\hat{m}\frac{\partial\tilde{\psi}}{\partial x} - \hat{k}\frac{\partial\tilde{\psi}}{\partial z}\right) + R_T\frac{\partial\tilde{\psi}}{\partial x} - H\frac{\partial\tilde{\psi}}{\partial z} = \nabla^2\tilde{T}, \tag{2.16b}$$

$$\frac{\partial\tilde{S}}{\partial t} + \hat{\psi}\sin(\hat{\boldsymbol{k}}\cdot\boldsymbol{x})\left(\hat{k}\frac{\partial\tilde{S}}{\partial z} - \hat{m}\frac{\partial\tilde{S}}{\partial x}\right) + \hat{S}\cos(\hat{\boldsymbol{k}}\cdot\boldsymbol{x})\left(\hat{m}\frac{\partial\tilde{\psi}}{\partial x} - \hat{k}\frac{\partial\tilde{\psi}}{\partial z}\right) + R_S\frac{\partial\tilde{\psi}}{\partial x} - H\frac{\partial\tilde{\psi}}{\partial z} = \tau\nabla^2\tilde{S}. \tag{2.16c}$$

These equations will have a solution that can be expressed in Floquet form:

$$(\tilde{\psi}, \tilde{T}, \tilde{S}) = \exp\{\lambda t + \mathrm{i}(kx+mz)\}\sum_{n=-\infty}^{\infty}(\psi_n, -\mathrm{i}T_n, -\mathrm{i}S_n)\exp(\mathrm{i}n\hat{\boldsymbol{k}}\cdot\boldsymbol{x}), \tag{2.17}$$

with ψ_n, T_n and S_n complex constants. Substituting into (2.16) we obtain the following set of real equations for each n:

$$\lambda\psi_n = -\sigma K_n^2\psi_n - \frac{\sigma(k+n\hat{k})}{K_n^2}T_n + \frac{\sigma(k+n\hat{k})}{K_n^2}S_n + \frac{(k\hat{m}-\hat{k}m)\hat{\psi}}{2K_n^2}[(K_{n-1}^2-\hat{\mu}^2)\psi_{n-1} - (K_{n+1}^2-\hat{\mu}^2)\psi_{n+1}\}, \tag{2.18a}$$

$$\lambda T_n = -K_n^2 T_n + [(k+n\hat{k})R_T - (m+n\hat{m})H]\psi_n + \tfrac{1}{2}(k\hat{m}-\hat{k}m)\hat{\psi}(T_{n-1}-T_{n+1}) + \tfrac{1}{2}(k\hat{m}-\hat{k}m)\hat{T}(\psi_{n-1}+\psi_{n+1}), \tag{2.18b}$$

$$\lambda S_n = -\tau K_n^2 S_n + [(k+n\hat{k})R_S - (m+n\hat{m})H]\psi_n + \tfrac{1}{2}(k\hat{m}-\hat{k}m)\hat{\psi}(S_{n-1}-S_{n+1}) + \tfrac{1}{2}(k\hat{m}-\hat{k}m)\hat{S}(\psi_{n-1}+\psi_{n+1}), \tag{2.18c}$$

where

$$K_n^2 = (k+n\hat{k})^2 + (m+n\hat{m})^2. \tag{2.18d}$$

Equations (2.18) can be expressed in terms of an infinite matrix

$$\lambda\boldsymbol{v} = \boldsymbol{A}\boldsymbol{v} \tag{2.19}$$

where $\boldsymbol{v}$ is the column vector $(\ldots, \psi_n, T_n, S_n, \psi_{n+1}, T_{n+1}, S_{n+1}, \ldots)$ and $\boldsymbol{A}$ an infinite matrix whose coefficients are obtained from (2.18*a–c*). In order to solve the stability problem the eigenvalues of a truncation of this matrix are found numerically, using routines from the NAG library. If the order of the matrix is sufficiently high then the eigenvalue with the largest real part will approximate those of the infinite system. This eigenvalue gives the growth rate of the fastest growing (or most slowly decaying) disturbance to the interleaving layers. The convergence of this eigenvalue can be tested by finding solutions for a range of truncations. In the subsequent work the truncation is chosen so that no significant variation is encountered when the order of the truncation is further increased.

In this paper we investigate the stability of the interleaving layers that occur when horizontal temperature and salinity gradients are present in a stratified fluid. The instabilities found all lie along the lines of minimum vertical density gradient. The instabilities are not particularly strongly influenced by the shear. They are driven principally by double diffusion, with modification due to the shear.

Dimensional quantities (compositional gradients, diffusivities etc.) are important in determining the physical sizes and growth rates of the interleaving layers (see Holyer 1983). However, once the layers are established, the quantities important for the formation and evolution of instabilities are non-dimensional; for example the ratio of the compositional gradients and the amplitude of the interleaving, which can be described in terms of, say, the ratio of the minimum to maximum vertical density gradients. The predictions of the analysis are also interpreted best in terms of non-dimensional quantities; for example the size of the instabilities compared to the background interleaving, or the growth rates compared to that of the fastest growing interleaving mode. Since it is in these terms that the instabilities can be best described, all subsequent discussion will concern non-dimensional quantities.

3. Investigation of stability

In this section we use the analysis set out in §2 to look at the stability of some particular examples of steady interleaving. One possible special case could be that of setting $H = 0$. This would recover the problem of the stability of salt fingers examined by Holyer (1984), whose results are reproduced when allowance is made for her use of the size of the salt finger with zero growth rate in her non-dimensionalizations, rather than the fastest growing fingers.

It is impractical to investigate the full range of parameters present in this problem with horizontal gradients present as there are too many degrees of freedom. Different fluids with different salts can take a wide range of values of σ and τ. Also, there are three independent salinity and temperature gradients to choose from, but it is the ratio of these that is important, and so there are effectively only two degrees of freedom in choosing the gradients. This can be seen from (2.11) where the three Rayleigh numbers are functions of two parameters only, the non-dimensional growth rate q and the ratio $\hat{m}/\hat{k}$ for the fastest growing mode. For the mode with zero growth rate that is parallel to this fastest growing mode we can have one last degree of freedom, the arbitrary amplitude $\hat{\psi}$. Hence the basic interleaving can be described by five independent parameters. We will restrict ourselves to investigating a subset of this parameter range in order to gain some insight into the driving mechanisms. First we consider only the case where $\sigma = 10$ and $\tau = 0.01$, the approximate values for common salt in water used by Holyer (1983). We will then look principally at two cases in some detail: (i) $R_T = 0$ (no background vertical temperature gradient), and

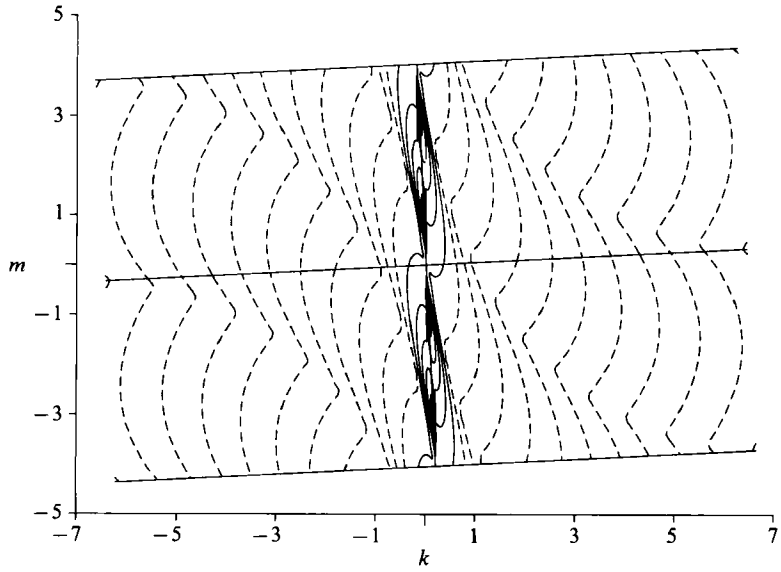

FIGURE 1. Contours of constant growth rate of the interleaving instability of Holyer (1983) for the case $R_T = 0$ with $q = \frac{7}{8}$. The contour interval is 0.2, with the zero and positive contours solid and negative contours dashed.

(ii) $R_S = 0$ (no background vertical salinity gradient). The former corresponds to the case where there are lateral temperature gradients imposed on a vertical salinity gradient (e.g. Chen *et al.* 1971; Thorpe *et al.* 1969; Tanny & Tsinober 1988) and the latter to the case where there is a compositional gradient imposed on thermally stratified fluid (e.g. Ruddick & Turner 1979).

In each of these cases we still have two free parameters to describe the interleaving state. One gives the ratio of the horizontal Rayleigh number to the non-zero vertical Rayleigh number, and the other the amplitude, $\hat{\psi}$, of the interleaving layers. For both cases (i) and (ii) instead of specifying the ratios of all the Rayleigh numbers it is convenient to specify the growth rate of the fastest-growing mode, q, and from this calculate the ratio $\hat{m}/\hat{k}$ and the remaining Rayleigh numbers.

In each case when the amplitude of the interleaving layers is set to zero we retrieve the stability problem that gave rise to the interleaving layers in the first place. As such the fastest growing mode is known. A typical plot of the non-dimensional growth rate as a function of the wavenumber of the disturbance is shown in figure 1 for the case $R_T = 0$ and $q = \frac{7}{8}$ (this corresponds to $R_S = -358.3$, $H = 70.43$ and $\hat{m}/\hat{k} = -19.32$). This shows the narrow band along the line in the $\hat{\boldsymbol{k}}$-direction where the modes are unstable. Also shown is the basic periodicity of the instabilities when expressed in Floquet form. The essential solutions remain unaltered if $\boldsymbol{k}$ is replaced by $-\boldsymbol{k}$, or if $\boldsymbol{k}$ is replaced by $\boldsymbol{k}+n\hat{\boldsymbol{k}}$ for any integer n.

As $\hat{\psi}$ is increased the picture changes. Figure 2 shows plots for (*a*) $\hat{\psi} = 0.096736$ and (*b*) $\hat{\psi} = 0.14$. In the former the fastest growing modes are no longer just those of the basic interleaving, but new modes are now present with the same growth rate. Since the modes whose wavenumber lies in the $\hat{\boldsymbol{k}}$-direction are parallel to the background interleaving layers there is no interaction through the nonlinear terms in the governing equations. Near this line there is little interaction and so the details are similar to those when $\hat{\psi} = 0$. Away from this line the growth rates are positive in the region of phase space shown (the extreme contours correspond to growth rate

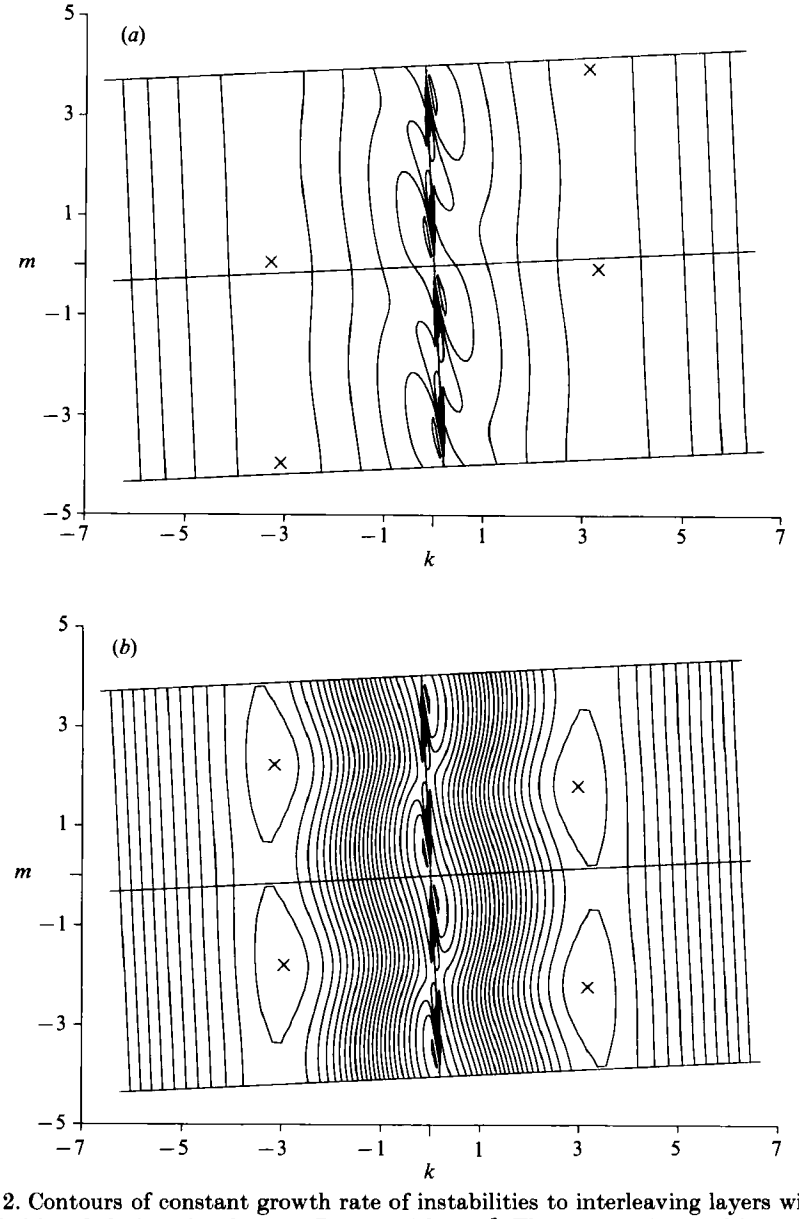

FIGURE 2. Contours of constant growth rate of instabilities to interleaving layers with amplitude (*a*) 0.096736 and (*b*) 0.14 for the case $R_T = 0$ with $q = \frac{7}{8}$. The contour interval is 0.2. The maxima shown by × have growth rates (*a*) 0.875 and (*b*) 4.721 respectively.

$\lambda = 0.2$). The growth rate rises to a maximum at a distance of just over 3 in wavenumber space from the line in the $\hat{k}$-direction through the origin. Along this ridge the variations in growth rate are relatively weak. When $\hat{\psi} = 0.14$, although the details very close to the line in the $\hat{k}$-direction are still similar to the case where $\hat{\psi} = 0$, the contours in growth rate are even more strongly dominated by the regions parallel to this axis with faster growing modes. These regions have peak values corresponding to growth rates of $\lambda = 4.721$, significantly bigger than $\frac{7}{8}$. Again the variation along this ridge in the growth rates are weak compared with the variations across it. Similar qualitative results are obtained for case (ii).

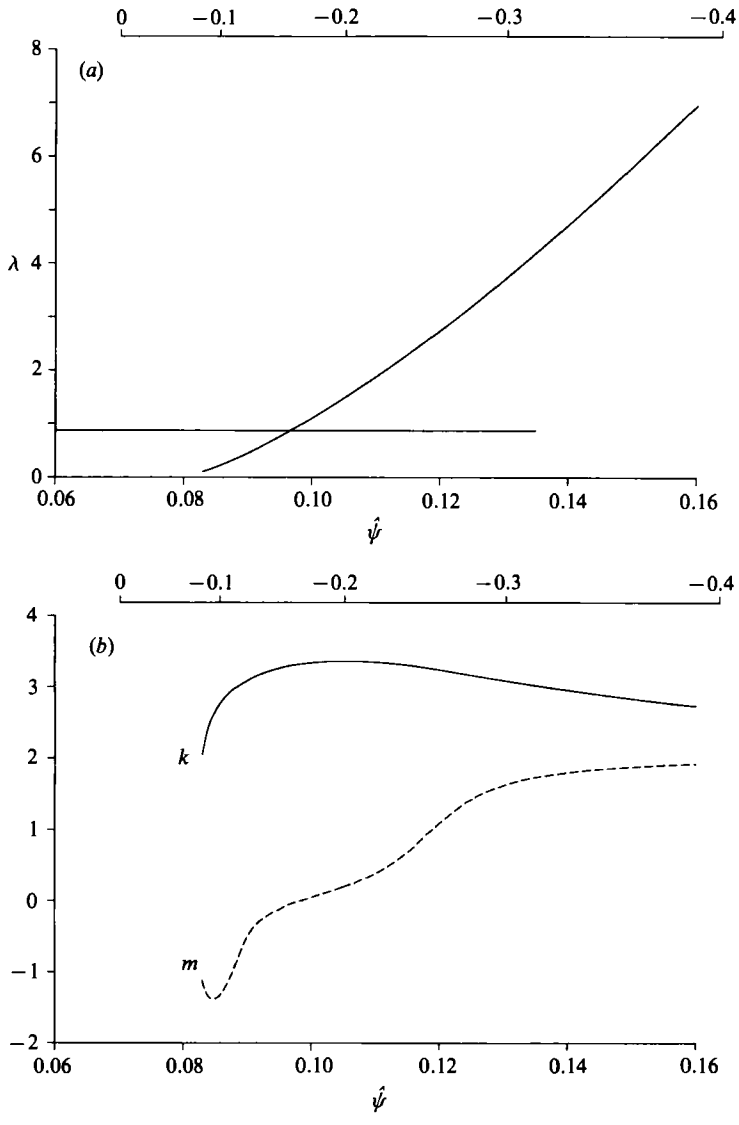

FIGURE 3. (*a*) The growth rate and (*b*) the wavenumber, $\boldsymbol{k} = (k, m)$, of the fastest growing instabilities for the case $R_T = 0$ with $q = \frac{7}{8}$ as functions of the amplitude of the interleaving layers, $\hat{\psi}$. The horizontal line in (*a*) shows the growth rate of the fastest growing interleaving mode, which is always unstable with growth rate $\frac{7}{8}$. In (*b*) the horizontal component of the wavenumber, k, is shown by the solid line, whilst the vertical component, m, is shown by the dashed line. In both graphs the ratio of the minimum density gradient to the maximum density gradient is shown along the top.

The variation in the fastest growing mode as a function of the interleaving amplitude, $\hat{\psi}$, is shown in figure 3, along with the wavenumbers of the fastest growing mode. The branch of fastest growing modes for high $\hat{\psi}$ ceases to be a global maximum when it crosses the line $q = \frac{7}{8}$; however, the branch of solutions continues to be a local maximum as shown. For this case the globally fastest growing mode is distinct from the fastest growing interleaving mode when there is a density inversion present in the fluid. It will be seen later that this is not always the case.

The form that such instabilities take is shown in figure 4. Since much of the detail

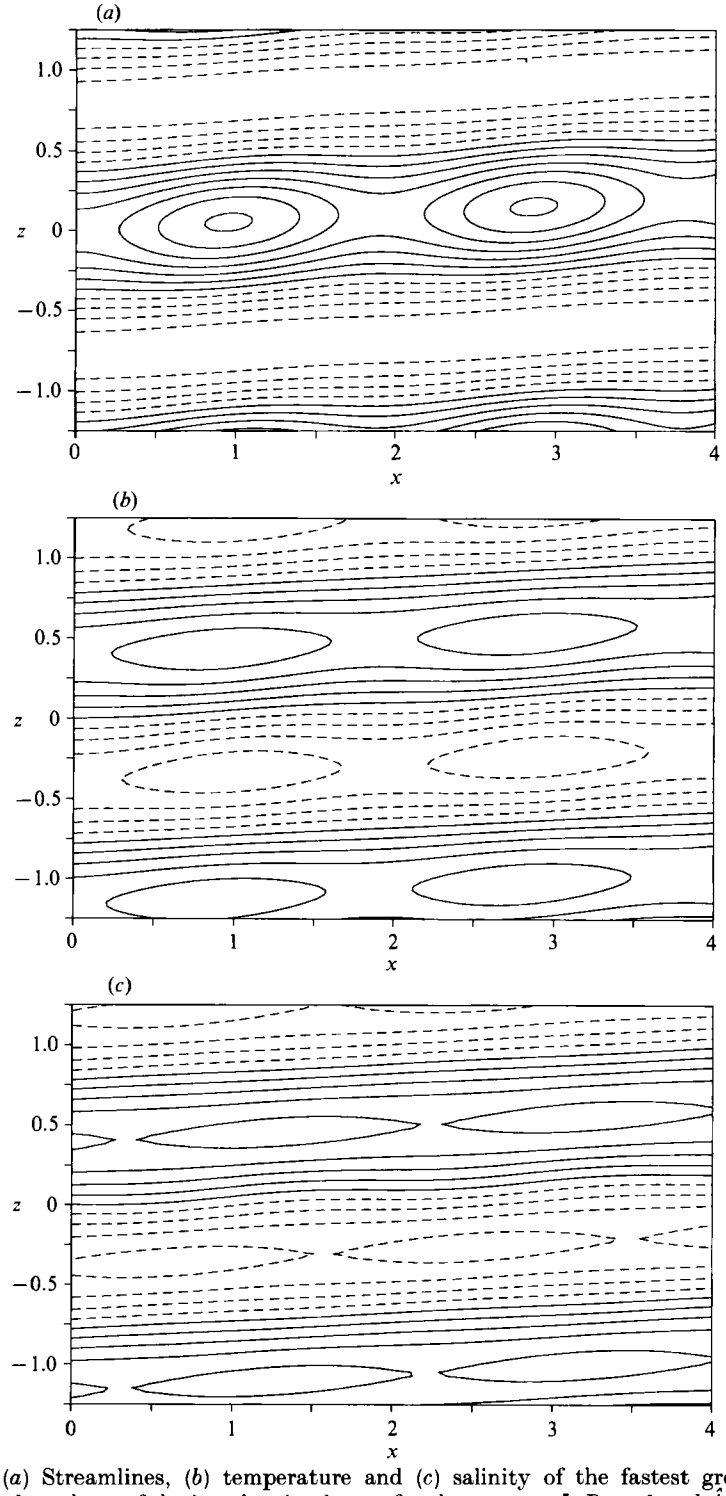

FIGURE 4. (*a*) Streamlines, (*b*) temperature and (*c*) salinity of the fastest growing instability superimposed on those of the interleaving layers for the case $q = \frac{7}{8}$, $R_T = 0$ and $\hat{\psi} = 0.096736$. The contour intervals are (*a*) 0.02, (*b*) 0.4, and (*c*) 30.0. The positive contours of the stream function in (*a*) are dashed, while the negative contours in (*b*) and (*c*) are dashed. In all cases the zero contour is solid.

of the streamlines occurs on the negative contours these are shown as solid lines and the positive contours as dashed lines. The streamlines show that convection cells form along the troughs in the interleaving stream function, whilst leaving the peaks relatively unaltered. The instabilities form in the regions of reduced vertical density gradients. However, the temperature and, more markedly, the salinity show relatively small perturbations from the background state. This could lead one to expect that these instabilities would be more noticeable if the flow in interleaving layers were visualized by means of some form of tracer in the fluid as opposed to using the shadowgraph technique. This conjecture is supported by the observations of Tsinober *et al.* (1983). In their figure 1 two simultaneous photographs were taken to show the convection due to a point source of heat in a salinity gradient. One used the shadowgraph technique and the other a tracer dye. The details of the convection inside the interleaving layers is almost undetectable in the shadowgraph, but shows up clearly when dye is used as a tracer. Numerous other examples exist in the published experiments where some dye or tracer particles are introduced into the fluid showing detail in the convecting layers that is invisible using the shadowgraph technique. In their observations Tanny & Tsinober used tracer particles suspended in the fluid. Long-exposure photographs of these particles clearly reveal instabilities in the convecting layers that bear a close resemblance to the streamlines of figure 4. In other cases the flow has been disclosed by dropping crystals of potassium permanganate through the fluid leaving vertical coloured streaks behind. These streaks then distort with the interleaving layers. It is often apparent that these streaks are smoother in the regions with enhanced vertical density gradients, and rougher in regions of diminished vertical gradients (see, for example, Thorpe, Hutt & Soulsby 1969; Chen, Paliwal & Wong 1976; Chen & Skok 1974; Tanny & Tsinober 1988).

These instabilities are driven principally by the temperature and salinity gradients in the interleaving layers, and not the shear. This can be seen by solving (2.18) with the terms involving $\hat{\psi}$ removed, while retaining the appropriate interleaving temperature and salinity perturbations. The contours of growth rate as a function of k are little changed, showing only a small reduction in the growth rates. Although there is an effect, it is destabilizing. Thus we are unlikely to have lost much significant information by restricting ourselves to two-dimensional instabilities and not allowing arbitrary three-dimensional disturbances for this case.

The analysis of the instability of finite-amplitude internal gravity waves (Mied 1976; Klostermeyer 1983) bears some similarity with the analysis presented here. However, the interpretation of the results of that analysis in terms of resonant triads is not applicable in this case. For small-amplitude internal waves the instabilities can be considered to be pairs of internal waves whose wavenumber vectors and frequencies sum to that of the principal internal wave. For instabilities of the double-diffusive interleaving we are looking at intrusions that are steady, and at instabilities with no imaginary part to their growth rate. As such there is no temporal resonance, and so a similar interpretation is not appropriate.

Similar results are found in the case $R_S = 0$. Here we have taken the case $q = \frac{1}{4}$ as an example (this corresponds to $R_T = 14.15$, $H = 2.335$ and $\hat{m}/\hat{k} = -3.470$). The fastest growing modes, and the corresponding wavenumbers, are shown in figure 5. A noticeable difference between this case and the previous one is that the growth rate of the instabilities exceeds that of the fastest growing interleaving layers when there are no density inversions in the background flow. This may be anticipated since the regions where the instabilities are centred have destabilizing vertical salinity

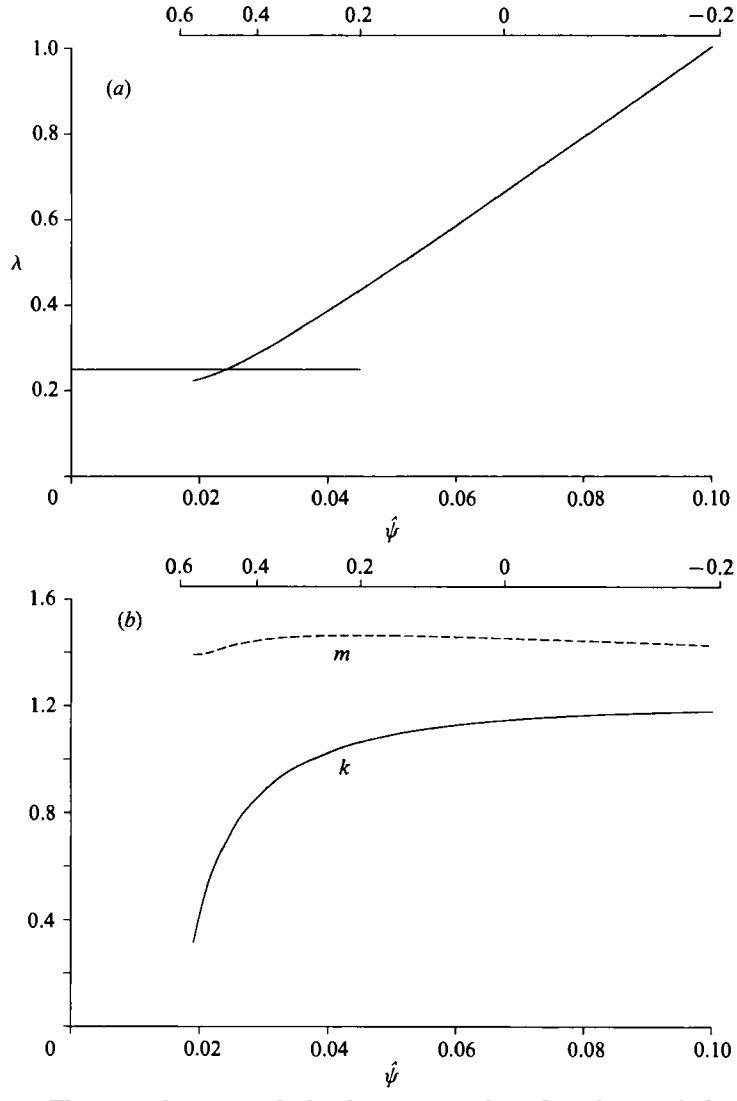

FIGURE 5. (*a*) The growth rate and (*b*) the wavenumber, $\boldsymbol{k} = (k, m)$, of the fastest growing instabilities for the case $R_S = 0$ with $q = \frac{1}{4}$ as functions of the amplitude of the interleaving layers, $\hat{\psi}$. The horizontal line in (*a*) shows the growth rate of the fastest growing interleaving mode, which is always unstable with growth rate $\frac{1}{4}$. In (*b*) the horizontal component of the wavenumber, k, is shown by the solid line, whilst the vertical component, m, is shown by the dashed line. In both graphs the ratio of the minimum density gradient to the maximum density gradient is shown along the top.

gradients due to the interleaving layers. Infinite fluids with destabilizing salinity gradients are prone to salt fingering if the stabilizing non-dimensional temperature gradient is less than a factor $1/\tau$ stronger than the destabilizing non-dimensional salinity gradient. Unlike the fully developed salt fingers frequently observed in experiments these instabilities are not particularly tall and thin, but are similar to marginally unstable salt fingers in a convecting layer in having an order-1 aspect ratio (Stern 1960).

We can look at how the onset of instability is affected as the relative horizontal background gradients vary. If we let ϵ be a measure of the ratio of the horizontal

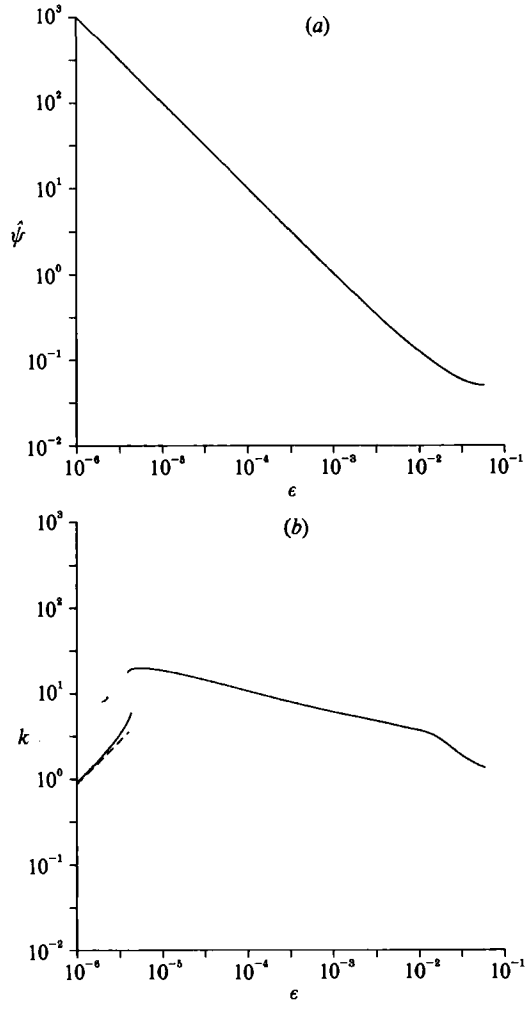

FIGURE 6. (*a*) The amplitude of interleaving, $\hat{\psi}$, and (*b*) the horizontal component of the wavenumber of the instability as functions of ϵ ($= H^{-1}$) for the case $R_T = 0$. These show the values for the fastest growing instability to the interleaving when it has the same growth rate as the most unstable interleaving mode. The dashed line in (*b*) shows the asymptotic limit for small ϵ. The corresponding line is plotted in (*a*) but is indistinguishable from the solid line.

gradients to the vertical gradients, whose definition is given below, it can be shown that as $\epsilon \to 0$ both the non-dimensional growth rate, q, and the vertical wavenumber, $\hat{m}$, of the background interleaving remain $O(1)$ whilst the horizontal component of the wavenumber, $\hat{k}$, is $O(\epsilon)$. From this it can be seen that R_T and R_S will both be $O(\epsilon^{-2})$ and H will be $O(\epsilon^{-1})$. It can also be shown that $\hat{T}$ and $\hat{S}$ will be a factor $O(\epsilon^{-1})$ larger than $\hat{\psi}$ in this small-ϵ limit.

We define the parameter ϵ to be the inverse of the horizontal Rayleigh number, H.

For a given ratio of the Rayleigh numbers the values of $\hat{\psi}$ and the horizontal wavenumber component, k, corresponding to the fastest growing modes for the case where their growth rate is equal to q can be found. Their behaviour as functions of ϵ are shown in figures 6 and 7 for the cases (i) $R_T = 0$ and (ii) $R_S = 0$ respectively. The ranges selected are those for which the horizontal gradients are weaker than the vertical gradient (i.e. $H < |R_T|$ or $H < |R_S|$ as appropriate). For these cases it is

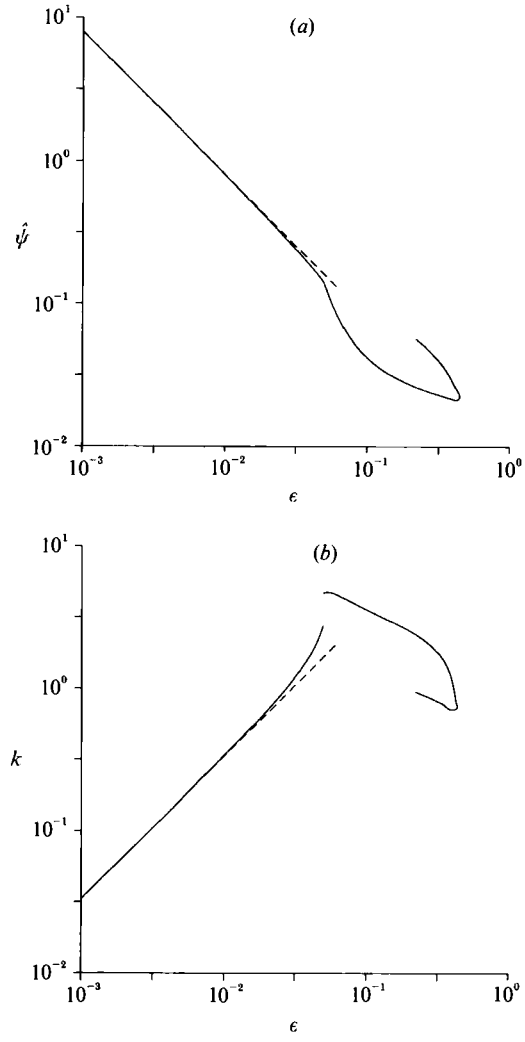

FIGURE 7. (*a*) The amplitude of interleaving, $\hat{\psi}$, and (*b*) the horizontal component of the wavenumber of the instability as functions of ϵ ($= H^{-1}$) for the case $R_S = 0$. These show the values for the fastest growing instability to the interleaving when it has the same growth rate as the most unstable interleaving mode. The dashed lines in (*a*) and (*b*) show the asymptotic limits for small ϵ.

possible for ϵ to take the same value for different ratios of the Rayleigh numbers and so in case (ii) the graphs of $\hat{\psi}$ and k as functions of ϵ are not single valued. This occurs when the background vertical and horizontal gradients are comparable, which is not the area of primary concern here. The other features are qualitatively similar. As ϵ initially decreases, so both $\hat{\psi}$ and k increase. At a specific value of ϵ the most unstable mode changes to another branch of solutions shown by the abrupt jump in k. The corresponding values of $\hat{\psi}$ change continuously, but with a discontinuity in the gradient of the curves, clearly visible in figure 7(*a*). After these critical points the curves settle down, with $\hat{\psi} \propto \epsilon^{-1}$ and $k \propto \epsilon$. In this limit the vertical lengthscale of the disturbances tends towards a fixed proportion the vertical scale of the background interleaving. The variation of m for the disturbances with maximal growth rates is not shown as there is little interdependency between the growth rates and m and so this is of little significance.

To investigate the asymptotic limit of small ϵ we rescale (2.16) using

$$t = t^*, \quad x = \epsilon^{-1}x^*, \quad z = z^*, \tag{3.1a–c}$$

$$H = \epsilon^{-1}, \quad R_T = R_T^*\epsilon^{-2}, \quad R_S = R_S^*\epsilon^{-2}, \tag{3.1d–f}$$

$$\hat{k} = \epsilon\hat{k}^*, \quad \hat{m} = \hat{m}^*, \tag{3.1g,h}$$

$$\hat{\psi} = \epsilon^{-1}\hat{\psi}^*, \quad \hat{T} = \epsilon^{-2}\hat{T}^*, \quad \hat{S} + \epsilon^{-2}\hat{S}^*, \tag{3.1i–k}$$

$$\tilde{\psi} = \tilde{\psi}^*, \quad \tilde{T} = \epsilon^{-1}\tilde{T}^*, \quad \tilde{S} = \epsilon^{-1}\tilde{S}^*. \tag{3.1l–n}$$

To leading order in ϵ the equations become, after dropping the asterisks,

$$\frac{1}{\sigma}\left[\frac{\partial^3\tilde{\psi}}{\partial t\partial z^2} + \hat{\psi}\sin(\hat{\boldsymbol{k}}\cdot\boldsymbol{x})\left\{\hat{k}\left(\frac{\partial^3\tilde{\psi}}{\partial z^3} + \hat{m}^2\frac{\partial\tilde{\psi}}{\partial z}\right) - \hat{m}\left(\frac{\partial^3\tilde{\psi}}{\partial x\partial z^2} + \hat{m}^2\frac{\partial\tilde{\psi}}{\partial x}\right)\right\}\right] = \frac{\partial\tilde{T}}{\partial x} - \frac{\partial\tilde{S}}{\partial x} + \frac{\partial^4\tilde{\psi}}{\partial z^4}, \tag{3.2a}$$

$$\frac{\partial\tilde{T}}{\partial t} + \hat{\psi}\sin(\hat{\boldsymbol{k}}\cdot\boldsymbol{x})\left(\hat{k}\frac{\partial\tilde{T}}{\partial z} - \hat{m}\frac{\partial\tilde{T}}{\partial x}\right) + \hat{T}\cos(\hat{\boldsymbol{k}}\cdot\boldsymbol{x})\left(\hat{m}\frac{\partial\tilde{\psi}}{\partial x} - \hat{k}\frac{\partial\tilde{\psi}}{\partial z}\right) + R_T\frac{\partial\tilde{\psi}}{\partial x} - \frac{\partial\tilde{\psi}}{\partial z} = \frac{\partial^2\tilde{T}}{\partial z^2}, \tag{3.2b}$$

$$\frac{\partial\tilde{S}}{\partial t} + \hat{\psi}\sin(\hat{\boldsymbol{k}}\cdot\boldsymbol{x})\left(\hat{k}\frac{\partial\tilde{S}}{\partial z} - \hat{m}\frac{\partial\tilde{S}}{\partial x}\right) + \hat{S}\cos(\hat{\boldsymbol{k}}\cdot\boldsymbol{x})\left(\hat{m}\frac{\partial\tilde{\psi}}{\partial x} - \hat{k}\frac{\partial\tilde{\psi}}{\partial z}\right) + R_S\frac{\partial\tilde{\psi}}{\partial x} - \frac{\partial\tilde{\psi}}{\partial z} = \tau\frac{\partial^2\tilde{S}}{\partial z^2}. \tag{3.2c}$$

For a given ratio of R_S and R_T we only have one free parameter describing the background state, the amplitude of the interleaving. As before, we solve this system by expressing the perturbation in Floquet form (2.17) and solve to find the form of the instability to the interleaving layers with zero growth rate. The background state is unstable to modes whose growth rate exceeds q when

$$\text{(i)}\, R_S = 0\text{:}\ \hat{\psi} = 7.94475\times10^{-3}, \quad k = 33.22, \qquad m = 1.126, \tag{3.3a}$$

$$\text{(ii)}\, R_T = 0\text{:}\ \hat{\psi} = 1.00374\times10^{-3}, \quad k = 8.865\times10^{5}, \quad m = 2.80. \tag{3.3b}$$

The growth rates of the fastest growing instabilities change rapidly for small changes in $\hat{\psi}$ for the case of $R_T = 0$, varying by more than one order of magnitude for variations in $\hat{\psi}$ of less than 1%. Those for the case $R_S = 0$ change more slowly, with modes of non-zero growth rate present near the above wavenumber even if $\hat{\psi} = 0$. Because of the sensitivity of the growth rate to the amplitude of the interleaving, we would expect instabilities in the case $R_T = 0$ to appear much more suddenly than in the case $R_S = 0$ where the transition to instability may be less well defined.

In both the above cases the instabilities first occur when fluid is stably stratified. The local Richardson number, defined by

$$Ri = -g\frac{\partial\rho}{\partial z}\Big/\left(\frac{\partial^2\hat{\psi}}{\partial z^2}\right)^2, \tag{3.4}$$

has local minima along the lines $\hat{\boldsymbol{k}}\cdot\boldsymbol{x} = n\pi$, taking the values

$$Ri = \sigma\frac{R_T - R_S \pm \hat{m}(\hat{T}-\hat{S})}{\hat{m}^4\hat{\psi}^2} = \sigma\frac{R_T - R_S \pm \hat{m}^5\hat{\psi}/\hat{k}}{\hat{m}^4\hat{\psi}^2}. \tag{3.5}$$

These values are independent of the rescaling involving ϵ. The smallest values of the Richardson number occur along the lines $\hat{\boldsymbol{k}}\cdot\boldsymbol{x} = 2n\pi$ where the instabilities are observed. The values that correspond to marginal stability are

$$R_T = 0, \quad Ri = 42590, \tag{3.6a}$$

$$R_S = 0, \quad Ri = 8.378. \tag{3.6b}$$

In both cases Ri is significantly greater than $\frac{1}{4}$ and so it is clear that the driving mechanism for instability is not that of shear. As before it is driven by double diffusion with modifications due to shear.

The double-diffusive mechanisms behind these instabilities can be understood by reference to figure 2 of Holyer (1983) for the case $R_S = 0$. If we look at the local salinity and temperature gradients that result from the presence of the interleaving then we can see that initially $\beta\bar{S}_z/\alpha\bar{T}_z = 0$ for $\hat{\psi} = 0$. Along the lines of $\hat{\boldsymbol{k}}\cdot\boldsymbol{x} = 2n\pi$ the local value of $\beta\bar{S}_z/\alpha\bar{T}_z$ increases as $\hat{\psi}$ increases. Since the horizontal gradients are weak compared to the vertical temperature gradient, $\beta\bar{S}_x/\alpha\bar{T}_z$ is effectively zero for the purpose of reference to Holyer's figure. In her figure 2(*a*) it can be seen that the fastest growing interleaving corresponding to these local gradients have a faster growth rate than those corresponding to the original gradients. Figure 2(*c*) shows that the value of R_T for the fastest growing mode decreases as $\beta\bar{S}_z/\alpha\bar{T}_z$ increases. This implies, since the local vertical temperature gradient is also increasing, that the lengthscale of the fastest growing instabilities is decreasing. In effect the regions along the lines $\hat{\boldsymbol{k}}\cdot\boldsymbol{x} = 2n\pi$ are becoming more unstable to interleaving instabilities of shorter lengthscales. It is these instabilities, modified by the shear, that evolve.

4. Conclusions

The growth rate of the instabilities was found to be weakly varying with changes in their wavenumber vector in the direction $\hat{\boldsymbol{k}}$, the wavenumber vector of the background interleaving. From this we can conclude that there is weak interaction between the instabilities that occur along one layer of local minimum density gradient and the next. This is not surprising as energy transfer between adjacent layers would be via internal waves. These waves would be absorbed at the critical layers along the lines of maximum density gradient where the velocity vanishes (Booker & Bretherton 1967), hence reducing communication between the regions of instability.

The rapidity of the growth rate of these instabilities in the case $R_T = 0$ (commonly used in experiments) after the onset of these instabilities would lead us to expect that these instabilities would be almost universal in experiments which involve the investigation of instabilities in salinity gradients. This rapidity may lead one to anticipate that a purely linear description of these instabilities would not be appropriate within a short period after the onset of instability.

We have examined the case where the fluxes of salt and heat are driven by molecular diffusivity. We have not looked at the models with fluxes driven by, for example, salt fingering. As such the results are only applicable to situations where salt fingering is not the dominant vertical mixing process, such as when there is no destabilizing vertical salinity gradient. When the effect of salt fingers dominates the fluxes of salt and heat other flux models are more appropriate (Stern 1967; McDougall 1985). If we model these fluxes by appropriate eddy diffusivities it would be expected that similar results to those found here would follow. However, incorporating the effects of shear and the nonlinearity of the flux laws for salt fingers would require a deeper analysis than is presented here.

We have restricted ourselves to two-dimensional instabilities. We have not considered possible instabilities that would result in a flow that is three-dimensional in its nature. Experimental observations of interleaving instabilities usually involve observations perpendicular to the horizontal gradients, and hence would tend not to show much evidence for three-dimensional disturbances. Those experimental

observations that are not perpendicular to the horizontal gradients are derived from situations with radial horizontal gradients and as such, have a more complicated three-dimensional structure than the basic interleaving. This structure would mask possible observations of any three-dimensional instabilities. When ϵ is small it may be anticipated that instabilities would appear aligned with the shear soon after the local vertical temperature and salinity gradients exceeded the criterion for the occurrence of double-diffusive instabilities. Although this criterion may be met before those for the two-dimensional instabilities studied here, the difference in amplitude of the interleaving required for the two criteria to be met is small and as such little difference will be made to the predictions for the onset of instabilities.

These instabilities will lead to enhanced mixing in the region of minimum (or reversed) vertical density gradient. This would lead to regions developing with greater uniformity of salinity and temperature. Such regions will be separated by regions with sharper vertical density gradients. These regions of sharper density gradients will show up more clearly when observations are made using the shadowgraph technique than the interior structure of the instabilities. This enhanced mixing will lead to the development of the step-like vertical density structure observed so frequently in the presence of double-diffusive interleaving.

REFERENCES

Booker, J. R. & Bretherton F. P. 1967 The critical layer for internal gravity waves in a shear flow. *J. Fluid Mech.* **27**, 513–539.

Chen, C. F., Briggs, R. A. & Wirtz, D. G. 1971 Stability of thermal convection in a salinity gradient due to lateral heating. *Intl J. Heat Mass Transfer* **14**, 57–65.

Chen, C. F., Paliwal, R. C. & Wong, S. B. 1976 Cellular convection in density stratified fluid: effect of inclination of the heated wall. *Proc. 1976 Heat Transfer & Fluid Mech. Inst.* 18–32. Stanford University Press.

Chen, C. F. & Skok, M. W. 1974 Cellular convection in a salinity gradient along a heated inclined wall. *Intl J. Heat Mass Transfer* **17**, 51–60.

Chen, C. F. & Sandford, R. D. 1977 Stability of time-dependent double-diffusive convection in an inclined slot. *J. Fluid Mech.* **83**, 83–95.

Hart, J. E. 1971 On sideways diffusive instability. *J. Fluid Mech.* **49**, 279–288.

Hart, J. E. 1973 Finite amplitude sideways diffusive convection. *J. Fluid Mech.* **59**, 47–64.

Holyer, J. Y. 1983 Double-diffusive interleaving due to horizontal gradients. *J. Fluid Mech.* **137**, 347–362.

Holyer, J. Y. 1984 Stability of long, steady two-dimensional salt fingers. *J. Fluid Mech.* **147**, 169–185.

Holyer, J. Y., Jones, T. J., Priestly, M. G. & Williams, N. C. 1987 The effect of vertical temperature and salinity gradients on double-diffusive interleaving. *Deep-Sea Res.* **34**, 517–530.

Huppert, H. E. & Josberger, E. G. 1980 The melting of ice in cold stratified water. *J. Phys. Oceanogr.* **10**, 953–960.

Huppert, H. E. & Turner, J. S. 1980 Ice blocks melting into a salinity gradient. *J. Fluid Mech.* **100**, 367–384.

Kerr, O. S. 1989 Heating a salinity gradient from a vertical sidewall: linear theory. *J. Fluid Mech.* **207**, 323–352.

Kerr, O. S. 1990 Heating a salinity gradient from a vertical sidewall: nonlinear theory. *J. Fluid Mech.* **217**, 529–546.

Kerr, O. S. 1991 Double-diffusive instabilities at a sloping boundary. *J. Fluid Mech.* **225**, 333–354.

Klostermeyer, J. 1983 Parametric instabilities of internal gravity waves in Boussinesq fluids with large Reynolds numbers. *Geophys. Astrophys. Fluid Dyn.* **26**, 85–105.

LINDEN, P. F. & WEBER, J. E. 1977 The formation of layers in a double-diffusive system with a sloping boundary. *J. Fluid Mech.* **81**, 757–773.

MCDOUGALL, T. J. 1985 Double-diffusive interleaving I. *J. Phys. Oceanogr.* **15**, 1532–1541.

MIED, R. P. 1976 The occurrence of parametric instabilities in finite-amplitude internal gravity waves. *J. Fluid Mech.* **78**, 763–784.

NARUSAWA, U. & SUZUKAWA, Y. 1981 Experimental study of double-diffusive cellular convection due to a uniform lateral heat flux. *J. Fluid Mech.* **113**, 387–405.

PALIWAL, R. C. & CHEN, C. F. 1980*a* Double-diffusive instability in an inclined fluid layer. Part 1. Experimental investigation. *J. Fluid Mech.* **98**, 755–768.

PALIWAL, R. C. & CHEN, C. F. 1980*b* Double-diffusive instability in an inclined fluid layer. Part 2. Stability analysis. *J. Fluid Mech.* **98**, 769–785.

POSMENTIER, E. S. & HIBBARD, C. B. 1982 The role of tilt in double-diffusive interleaving. *J. Geophys. Res.* **87**, 518–524.

PROCTOR, M. R. E. 1981 Steady subcritical thermohaline convection. *J. Fluid Mech.* **105**, 507–521.

RUDDICK, B. R. & TURNER, J. S. 1979 The vertical length scale of double-diffusive intrusions. *Deep-Sea Res.* **26**, 903–913.

STERN, M. E. 1960 The 'salt fountain' and thermohaline convection. *Tellus* **12**, 172–175.

STERN, M. E. 1967 Lateral mixing of water masses. *Deep-Sea Res.* **14**, 747–753.

TANNY, J. & TSINOBER, A. B. 1988 The dynamics and structure of double-diffusive layers in sidewall-heating experiments. *J. Fluid Mech.* **196**, 135–156.

THANGAM, S., ZEBIB, A. & CHEN, C. F. 1982 Double-diffusive convection in an inclined fluid layer. *J. Fluid Mech.* **116**, 363–378.

THORPE, S. A., HUTT, P. K. & SOULSBY, R. 1969 The effects of horizontal gradients on thermohaline convection. *J. Fluid Mech.* **38**, 375–400.

TOOLE, J. M. & GEORGI, D. T. 1981 On the dynamics and effects of double-diffusively driven intrusions. *Prog. Oceanogr.* **10**, 123–145.

TSINOBER, A. B., YAHALOM, Y. & SHLIEN, D. J. 1983 A point source of heat in a stable salinity gradient. *J. Fluid Mech.* **135**, 199–217.

WIRTZ, R. A., BRIGGS, D. G. & CHEN, C. F. 1972 Physical and numerical experiments on layered convection in a density-stratified fluid. *Geophys. Fluid Dyn.* **3**, 265–288.